A numerical strength prediction approach for wood using element-wise local fiber directions from laser scanning

Seeber, Franziska ; Sarnaghi, Ani Khaloian; Rais, Andreas; van de Kuilen, Jan-Willem

DOI
10.1016/j.matdes.2022.111578

Publication date
2023

Document Version
Final published version

Published in
Materials & Design

Citation (APA)
Seeber, F., Sarnaghi, A. K., Rais, A., & van de Kuilen, J.-W. (2023). A numerical strength prediction approach for wood using element-wise local fiber directions from laser scanning. *Materials & Design*, *226*, Article 111578. https://doi.org/10.1016/j.matdes.2022.111578

Materials & Design 226 (2023) 111578

Contents lists available at ScienceDirect

Materials & Design

journal homepage: www.elsevier.com/locate/matdes

A numerical strength prediction approach for wood using element-wise local fiber directions from laser scanning

Franziska Seeber [a,*], Ani Khaloian-Sarnaghi [a], Andreas Rais [a], Jan-Willem van de Kuilen [a,b]

[a] Technical University of Munich, TUM School of Engineering and Design, Department of Materials Engineering, Winzererstrasse 45, München 80797, Germany
[b] Delft University of Technology, Faculty of Civil Engineering and Geosciences, Biobased Structures and Materials, Stevinweg 1, Delft 2628 CN, the Netherlands

HIGHLIGHTS

- 3D orthotropic model, based on fiber angles from laser scanning of board surfaces.
- Data-driven FE model, representing the stiffness variation of European beech boards.
- Stress distributions in boards follow the imperfections of boards.
- Normal/shear stress components from simulations are good tensile strength predictors.

GRAPHICAL ABSTRACT

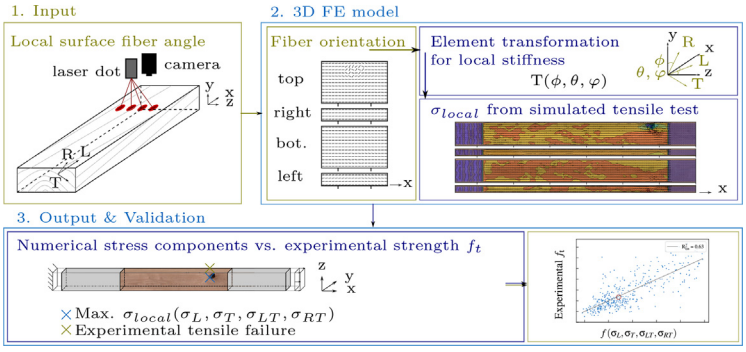

ARTICLE INFO

Article history:
Received 1 July 2022
Revised 16 December 2022
Accepted 31 December 2022
Available online 5 January 2023

Keywords:
Laser scanning
FE model
3D stresses
Virtual strength prediction

ABSTRACT

Mechanical properties of wood such as stiffness and strength vary locally especially due to heterogeneities and anisotropy. Analytical models and numerical simulations of wooden boards are able to represent varying material orientation e.g. with local fiber directions from laser scanning as input for the prediction of strength. Current Finite Element Models reconstructed the grain orientation by means of computationally demanding fluid analysis around obstacles like knots; whereas the available fiber pattern, captured by means of laser scanning, was passed solely into the detection of knots, but not directly processed for the inclusion of material fiber orientation. Therefore, the goal of this paper was the development of a numerical approach to directly include locally varying measured fiber orientation with orthotropic material properties and to predict the tensile strength of boards with reduced computational effort. Therefore, the stiffness was transformed element-wise according to the measured fiber deviations and the local fiber stress components were computed for the specific tensile load case. For the virtual strength prediction, numerical maximum stress values were compared to experimental tensile strength. Good agreements were observed with reduced computational effort compared to existing approaches between numerical and experimental results.

1. Introduction

Understanding the mechanical behavior of wood is fundamental for optimizing wood products, such as glulam, and accordingly to improve building structures. Wood is a naturally grown fiber-based composite material characterized by heterogeneities and

* Corresponding author.
E-mail address: seeber@hfm.tum.de (F. Seeber).

https://doi.org/10.1016/j.matdes.2022.111578
0264-1275/

orthotropic material properties. Knots represent heterogeneities and consequently the fiber orientation deviates from the boards global coordinate system. Furthermore, the local orthotropic stiffness differs in magnitudes according to its direction parallel or perpendicular to the fiber. All, heterogeneities, the orthotropic material properties, and a differentiation for wood species, are fundamental for specifying the mechanical behavior of wood under physical loading.

Different methods were developed for the assessment of fiber direction on boards first for softwood and lately also for hardwoods: Laser scanning and the resulted scatter in light due to the tracheid effect is one existing approach, which is investigated in [1,2] and used also in industry [3]. Due to the light scatter of a laser dot on the board surface, an ellipse is formed. Consequently, the angle between the major axis of the ellipse and the longitudinal board axis presents the fiber direction. In addition to laser scanning, approaches exist to detect the fiber direction based on thermal conductivity [4], microwave scanning [5] or electric field strength measurement [6]. Another approach on European beech boards considers the analysis of medullary rays on transverse planes for the determination of the fiber direction of European beech boards [7]. Recent research also used X-ray computed tomography scans for the estimation of the fiber direction around knots [8,9].

The convenience of grain deviation information is shown in various aims in the literature: either as estimator of strength, as Indicating Property (IP) for machine grading or for simulation of the mechanical behavior in the anisotropic material with imperfections. The transformation between global and local fiber orientation was introduced in studies, such as the work of [10]. In [11,12], an analytical model is developed to rotate the stiffness locally depending on the laser scanning grain orientation. In such an approach, the horizontal and the vertical angles are distinguished according to the measured fiber pattern over the surfaces and interpolated into the thickness of the boards [13,14]. Additionally, the pith is included in the aforementioned model [12] and adapted along the board [15,16]. Further studies focus on the determination of the diving angle according to the ellipse ratio [17]. With the analytical model, developed in [12], the local bending modulus of elasticity based on the grain orientation can be used as an identifying parameter for the prediction of bending strength [12,14].

Other approaches establish and investigate the slope of grain (SOG) [18,19] based on laser scanning fiber direction. In [19], the three-dimensional averaged grain angle in sections of 150 mm along the board are calculated to represent knots and knot clusters with its varying fiber deviation. Accordingly, the amount of inhomogeneity is defined in the board and the tensile strength can be predicted without considering the mechanical behavior of the boards under stress.

Numerical approaches utilize the fiber orientation from laser scanning as input data for the reconstruction of knot locations for Finite Element Models [20]. However, the fiber pattern around knots is represented according to mathematical equations based on the 3D flow grain analogy in [21]. The flow grain analogy was first established for describing the fiber pattern in wood [22,23]. Potential streamlines of fluid in such approach are passing around an obstacle in the 2D longitudinal-tangential board and thus represent the assumed laminar grain pattern.

In recent years considerable research was conducted on numerical models for predicting the stiffness of boards with heterogeneities under tensile or bending stresses based on simulations of fluid streamlines representing the fiber pattern [24–27]. The mechanical behavior and failure of boards with a single knot was analyzed in literature considering trajectories of laminar streamlines in 3D for grain orientation [24,25]. Concurrently, [26] modeled the grain orientation based on the principal stress theory and compared it to fluid analysis approaches.

In [27], boards were modeled by considering the actual geometrical coordinates of multiple knots. Knots were reconstructed as cones or cylinders, taken as holes in the board and Computational Fluid Dynamics (CFD) analysis was used to model the grain orientation based on turbulent flow. Similarly, in the studies of [28], knots were included as cones into the FE model of boards based on their geometrical coordinates. Further studies [29,20] developed knot recognition algorithms to detect and include knots in the models. Developments in the numerical modeling considered the inclusion of pith, and provided an improved model for the prediction of fiber pattern [30]. The validation of aforementioned numerical models was mainly done by experimental results such as strength values or strain values, measured by strain measurement devices such as Digital Image Correlation (DIC) systems.

In grading, strength prediction is conducted using IPs based on either visual grading parameters such as knot geometry, size, and location or machine grading parameters such as density, dynamic modulus of elasticity (E_{dyn}), and knot recognition parameters. Local material properties are thus assessed as IPs or expressed in forms of local bending modulus of elasticity [14], 3D slope of grain (SOG_{3D}) [19] or stress concentration factors [27] ect. for strength prediction. Whereas for softwoods, the size of knots, fiber deviation and the E_{dyn} are relatively good single tensile strength predictors, this is slightly different for hardwoods e.g. beech or tropical hardwoods, since this relates more to the tree structure and the part of the log that the board is cut from [7,31–33].

The assessment of mechanical properties of boards taking into account the local material directions in FE models solely based on fiber deviation data from laser scanning is not analyzed in literature. Thus, this study focuses on the implementation of the measured fiber angle data from laser scanning directly as input data for the estimation of local material directions in FE models and further to process the model for extraction of numerical parameters for prediction of strength. The objective is an approach for better numerical representation of wood with its heterogeneities, and anisotropy to improve the quality of strength predictions. The established model provides a basis for developments with the aim to further analyze failure initiation and propagation.

2. Material and method

2.1. Material properties

This study concerned 407 boards from 100 European beech *Fagus sylvatica* L. trees grown in Spessart in the middle of Germany near Frankfurt a.M. [19]. The dimensions of the boards after grading, sawing and planing were $38 \times 129 \times 2400\,mm^3$. The selection of the boards, in [19], covered a wide range of qualities with varying strength, stiffness and knottiness properties. Test results and the summary of material properties are presented in Table 1. Machine grading data, including fiber deviation measurement, the density and E_{dyn}, besides the visual grading data, describing the knots, were available for this dataset. For hardwood, especially European beech, fiber deviation might be more decisive than for softwood, due to the lack of clear identification of regular defects as e.g. knots [19]. Being a diffuse porous hardwood species, European beech has lower density variation compared to softwood or other ring-porous hardwood species, as shown in [34], which makes the distinction between clear wood and knots even more complex.

Additionally, experimental tensile tests were conducted on all samples, according to [35,36], on the weakest test length of nine times the width of the board. The static elastic modulus (E_{stat})

Table 1
Average testing and grading data. (Standard deviation given in brackets.)

n	length [mm]	thickness [mm]	width [mm]	ρ [kg/m^3]
407	2414 (5)	38.0 (0.2)	129.3 (0.8)	689 (33)

	E_{dyn} [N/mm^2]	E_{stat} [N/mm^2]	$f_{t,exp}$ [N/mm^2]	$u_{12\%}$ [%]
	15,110 (2180)	15,040 (2860)	53.8 (29.9)	9.9 (1.3)

and strength ($f_{t,exp}$) as well as information about the type and position of failure were obtained from the experimental tests. This experimental dataset is furthermore used to validate the numerical simulation approach presented in Section 2.3.

2.2. Laser scanning data and grain orientation

The surface projection of the longitudinal orthotropic material directions for the local fiber coordinate systems (local FCS) are determined by the industrial laser scanner Goldeneye (Microtec, Bressanone, Italy) on each of the surfaces of the boards. Based on the tracheid effect of wood, the light transmission of a laser dot through wooden cells is stronger in fiber direction than across the fiber. Consequently, the circular laser dot is reshaped into an ellipse and indicates the angle between the major axis of the ellipse, which allows determining the longitudinal axis of the board. All beech boards are scanned on four faces and processed longitudinally. Laser dots are determined with a scanning resolution of one laser dot per 1 mm in longitudinal direction and 4 mm in transverse direction. Accordingly, different fiber angles are determined on both wide and narrow faces of the boards [37] as shown in Fig. 1. The horizontal fiber angle on the wide faces of the board describes the in-plane angle θ and the vertical diving angle on the narrow faces of the board describes the out-of-plane angle φ. The ring angle ϕ is not measured, as the information about the pith location would be restricted to the two end-grain surfaces of the boards with an assumed linear pith over the length of the board. Since straight pith assumption can not be considered for beech wood, the ring angle is kept constant, with 0°, in the numerical model presented in Section 2.3. By means of linear interpolation between the data of two surfaces (top–bottom, left–right) an estimation is made for fiber angles inside the boards.

Laser scanning information gives a consistent representation of the fiber pattern over the surfaces of every single board, for which the presented material properties in Table 2 are assigned in the simulation. Thereby, based on the measured fiber angle, the orthotropic material stiffness is rotated point-wise and a local unidirectional orthogonal stiffness is assigned to the boards. Consequently, depending on the amount of rotation and on the elastic moduli in different directions, the tensile stiffness with respect to the global loading condition is reduced or increased.

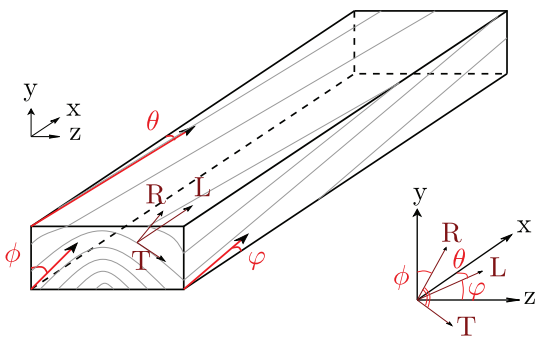

Fig. 1. Local fiber coordinate system with LRT (longitudinal, radial and tangential direction) on a board with global orientation x,y,z. The horizontal fiber angle θ, the vertical diving angle φ both obtained from laser scanning and the ring angle ϕ are shown.

In order to validate this detailed input data for numerical models, three main fiber zones, depending on the absolute magnitude of the fiber angle, are defined and compared to softwood in accordance with [30]: the knot zone (i), the fiber deviation zone (ii) and the clear wood zone (iii). In difference to softwood, knots appear more irregularly structured in European beech boards and further lack of clear identification due to its lower density variation as the coefficients of variation (COVs) for density are relatively low, seen in a large number of studies in beech [19]. A modest amount of knots, as well as large areas without knots but still decisive local fiber deviation, are common phenomena for this wood species. Thus, fiber deviation is considered an important feature. Two example boards are shown in Fig. 2: The schematic image and the fiber angles are presented on the left side for a board with knot, and on the right side the same data is shown for a board without knots.

The knot zone (i) is characterized by fiber angles between $\sim 55° - 90°$, outlined by red colors in Fig. 2b. This zone is identified by strong fiber deviation where the local FCS deviates strongly from the global board direction. An example knot zone area of a relatively regular-shaped knot is shown in Fig. 2 on the left side. Thereby, the knot area is emphasized by the red contour lines with a fiber angle higher than $\sim 55°$. Although this area in the selected example knot in Fig. 2 is small, it considerably influences the fiber pattern around the knot. Moreover, it needs to be considered that measurements inside a knot can scatter as presented with the color difference and tangled fiber distribution in Fig. 2b.

The fiber deviation zone (ii) can be characterized by fiber angles between $10° - 55°$, presented by yellow colors in Fig. 2b. This zone represents areas around knots with high fiber deviation, which indeed occur in boards with knots or also in boards without knots. In rectangularly truncated knots, as shown in Fig. 2, four peaks around the knot zone represent the horizontal fiber deviations with respect to the longitudinal board direction. Such areas with its local FCS, deviating from the global board directions, have an impact on the global stress distribution. The size of this region is influenced by the geometrical configuration and by the amount of knots.

The "clear wood" zone (iii) is characterized by fiber angles between $0° - 10°$, outlined by blue colors in Fig. 2b. This zone represents the natural fiber distribution in regions without knots. The local FCSs of this region are approximately in line with the global coordinate system.

Due to an irregular appearance of knots and wood defects, scattering laser angle measurements inside knots, as well as the unclear transition of knots to the surrounding wood, size and location of knots are more complex in hardwood than in softwood. Fur-

Table 2
Elastic material properties for European beech [38] in [N/mm²].

E_L	E_R	E_T	ν_{LR}	ν_{LT}	ν_{RT}	G_{LR}	G_{LT}	G_{RT}
14000	2280	1160	0.43	0.58	0.31	1640	1080	470

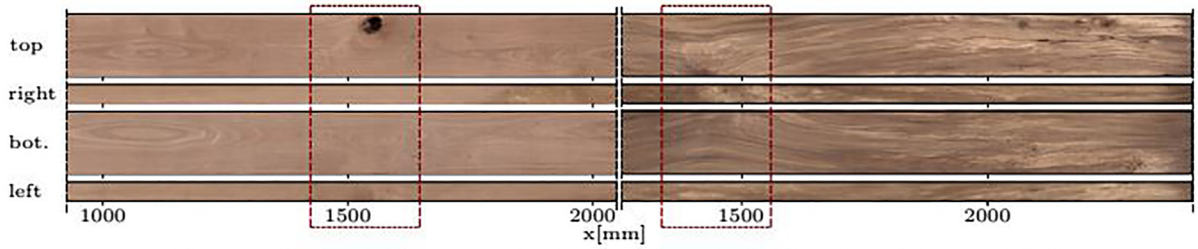

(a) Schematic image of board with knot (left) and board without knot (right).

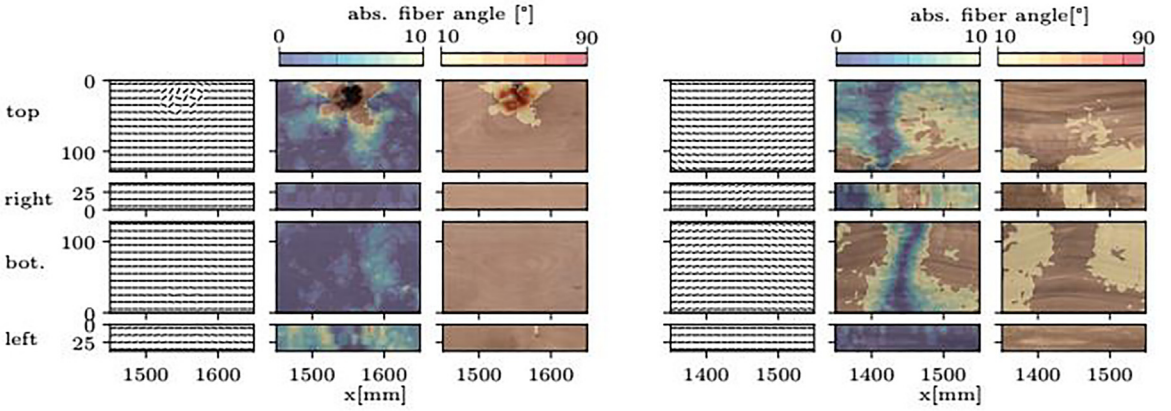

(b) Fiber angles in knot, fiber deviation and clear wood zone with focus on representative areas.

Fig. 2. Schematic image and fiber pattern on board surfaces. Fiber orientation based on laser scanning information on an example board with knot (left) and on an example board without knot (right).

thermore, fiber deviations lead to failure, as stated in [31]. Thus, the local fiber deviation regions around knots are the focus of this study and are taken as the only decisive input properties for the numerical model. The assumption of constant initial material properties, shown in Table 2 in all zones is made as input data for simulation, however, the model is also adapted to assign for different local material properties.

2.3. Numerical modeling

The main focus of this paper is to develop a numerical approach for direct implementation of the fiber pattern from laser scanners into a numerical model and to establish a prediction approach for tensile strength. Based on the discretized local fiber orientation, the orthotropic stiffness can be constructed locally. Local stiffness in the FCS, especially around knots, causes localization of global stress that may identify the location for failure initiation. The developed approach enables the simulation of the elastic mechanical behavior of specific wooden boards under tensile loading, however the approach is also extendable for bending cases. Consequently, maximum (normal and shear) stress components and their locations are investigated in this study.

The 407 beech boards, described in Section 2.1, are automatically numerically reconstructed and discretized by means of uniform regular solid elements. Brick solid elements with approximate size of 15mm × 15mm × 15mm and 8 integration points are used for the simulations. The uniform mesh without local refinements is chosen to capture the details of the fiber pattern from the laser scan resolution accuracy introduced in Section 2.2 and at the same time computational effort is kept relatively small.

The boundary conditions of the model are adapted to the experimental tension test as schematically presented in Fig. 3. According to the experimental test set-up in EN 408 [35], the test length is defined with 9 × width and shown in Fig. 3 and Fig. 4. Simplified, one side of the board is clamped, where all Degrees of Freedom (DoFs) are constrained. On the other side a nominal tensile stress of 1 MPa is applied in global x-direction. Due to the low tensile stress applied in the simulations, the material behavior remains in the linear elastic range.

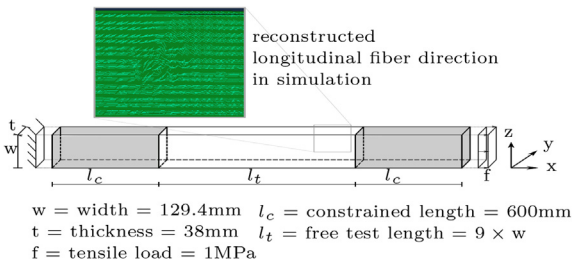

Fig. 3. Experimental tensile test setup with corresponding dimensions according to EN 408 [35] with illustrative reconstructed longitudinal fiber direction.

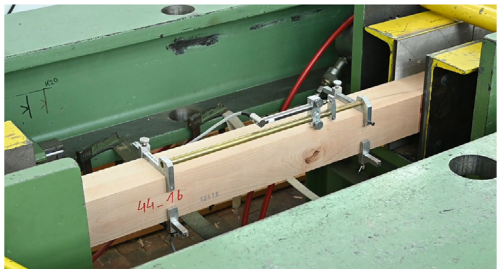

Fig. 4. Tensile testing device according to EN 408 [35].

Orthotropic material properties [38] are summarized in Table 2 and applied for the assumed linar elastic constitutive law,

$$\boldsymbol{\sigma} = \mathbf{C}\boldsymbol{\varepsilon}, \tag{1}$$

with $\boldsymbol{\sigma}$ as the stress tensor, $\mathbf{C}$ representing the orthotropic stiffness matrix and $\boldsymbol{\varepsilon}$ the strain tensor.

The local stiffness is defined by rotation of the orthotropic material properties based on local fiber directions, where radial and tangential directions are kept constant with a ring angle of 0° as discussed previously.

$\mathbf{T}_{z,\phi}, \mathbf{T}_{y,\theta}, \mathbf{T}_{x,\varphi}$ are the transformation matrices and represent the rotation around each axes x, y, z, respectively, as shown in Fig. 1.

$$\mathbf{T}_{\mathrm{x},\varphi} = \begin{bmatrix} 1 & 0 & 0 & 0 & 0 & 0 \\ 0 & c_\varphi^2 & s_\varphi^2 & 2c_\varphi s_\varphi & 0 & 0 \\ 0 & s_\varphi^2 & c_\varphi^2 & -2c_\varphi s_\varphi & 0 & 0 \\ 0 & -c_\varphi s_\varphi & c_\varphi s_\varphi & c_\varphi^2 s_\varphi^2 & 0 & 0 \\ 0 & 0 & 0 & 0 & c_\varphi & -s_\varphi \\ 0 & 0 & 0 & 0 & -s_\varphi & c_\varphi \end{bmatrix}, \begin{matrix} s_\varphi = sin(\varphi) \\ c_\varphi = cos(\varphi) \end{matrix} \tag{2}$$

$$\mathbf{T}_{\mathrm{y},\theta} = \begin{bmatrix} c_\theta^2 & 0 & s_\theta^2 & 0 & 2c_\theta s_\theta & 0 \\ 0 & 1 & 0 & 0 & 0 & 0 \\ s_\theta & 0 & c_\theta & 0 & -2c_\theta s_\theta & 0 \\ 0 & 0 & 0 & c_\theta & 0 & -s_\theta \\ -c_\theta s_\theta & 0 & c_\theta s_\theta & 0 & c_\theta^2 - s_\theta^2 & 0 \\ 0 & 0 & 0 & s_\theta & 0 & c_\theta \end{bmatrix}, \begin{matrix} s_\theta = sin(\theta) \\ c_\theta = cos(\theta) \end{matrix} \tag{3}$$

$$\mathbf{T}_{\mathrm{z},\phi} = \begin{bmatrix} c_\phi^2 & s_\phi^2 & 0 & 0 & 0 & 2c_\phi s_\phi \\ s_\phi^2 & c_\phi^2 & 0 & 0 & 0 & -2_\phi s_\phi \\ 0 & 0 & 1 & 0 & 0 & 0 \\ 0 & 0 & 0 & c_\phi & -s_\phi & 0 \\ 0 & 0 & 0 & s_\phi & c_\phi & 0 \\ -c_\phi s_\phi & c_\phi s_\phi & 0 & 0 & 0 & c_\phi^2 - s_\phi^2 \end{bmatrix}, \begin{matrix} s_\phi = sin(\phi) \\ c_\phi = cos(\phi) \end{matrix} \tag{4}$$

Therefore, the transformation matrix $\mathbf{T}_\sigma$ at each material point can be represented [39]:

$$\mathbf{T}_\sigma = \mathbf{T}_{\sigma,\varphi}\mathbf{T}_{\sigma,\theta}\mathbf{T}_{\sigma,\phi}. \tag{5}$$

The global stress $\boldsymbol{\sigma}_{\mathrm{glob}}$ as well as the stiffness tensor $\mathbf{C}$ is transformed between local and global coordinate systems by means of the transformation matrix:

$$\boldsymbol{\sigma}_{\mathrm{glob}} = \mathbf{C}\boldsymbol{\varepsilon}_{\mathrm{glob}} = \mathbf{T}_\sigma^{\mathrm{T}}\mathbf{C}\mathbf{T}_\sigma\boldsymbol{\varepsilon}_{\mathrm{loc}}, \tag{6}$$

$$\boldsymbol{\sigma}_{\mathrm{loc}} = \mathbf{C}_{\mathrm{loc}}\boldsymbol{\varepsilon}_{\mathrm{loc}}, \tag{7}$$

similar to the approach presented in [10,11,8].

The local stresses $\boldsymbol{\sigma}_{\mathrm{loc}}$ in the FCS (shown in Fig. 1) with the longitudinal stress component σ_L, the radial stress component σ_R, the tangential stress component σ_T, and the shear stress components $\sigma_{LR}, \sigma_{LT}, \sigma_{RT}$ and strains $\boldsymbol{\varepsilon}_{\mathrm{loc}}$ in corresponding local directions are calculated using Equ. (7).

The workflow is presented in Fig. 5. It is fully automated and various geometries as well as other material properties for different wood species can be assigned. The preprocessing of the input data and the geometrical construction of the FE model is done in Python (3.8). To include the fiber angles in the model, each integration point is linked with its nearest neighbor local FCS from the measured laser scanning data. Subsequently, the user-subroutine ORIENT in ABAQUS/Standard (Simulia 6.14, from Dessault Systems) is used as a tool to create and assign local FCSs on the integration points of every finite element. Within this process, also the mesh size can be adapted to an accuracy of the input data. Subsequently the stress analysis is run in ABAQUS and postprocessed in Python as described in Fig. 5.

2.4. Strength prediction and validation of numerical analysis

Experimental strength, elastic stiffness and failure locations from tensile tests are used as validation parameters for the numerical analysis. The stress distribution, varying locally due to deviations in fiber pattern, is studied in each single board. Maximum stress components, occurring in the boards, are then evaluated individually according to the direction of the local FCS. Normal and shear stress components are analyzed and the correlation between local maximum stress and experimental strength is investigated through single and multiple regression analysis. In this way, the virtual strength prediction of beech based on laser scanning data and numerical simulations is realized.

The approaches from two comparable studies, Khaloian et al. in [27] and Rais et al. in [19], are used on the dataset described in Section 2.1 to verify the numerical results and the developed prediction method.

Rais et al. computes the slope of grain $\mathrm{SOG}_{3\mathrm{D}}$ by Equ. (8), referencing to [37].

$$cos(\mathrm{SOG}_{3\mathrm{D}}) = cos(\theta_{in-plane}) \cdot cos(\varphi_{out-of-plane}) \tag{8}$$

Subsequently, the averaged slope of grain angle over 150 mm sections spots the weakest area of the boards without performing any mechanical analysis. This statistical analysis is performed in the current study for the same samples. The strength prediction based on $\mathrm{SOG}_{3\mathrm{D,150mm}}$ is investigated in comparison to the presented model for the validation of the results introduced in Section 3.1.

The second model, used for comparison and validation, includes numerical simulations for strength prediction based on visual surface measurement data [27]. Based on geometrical coordinates, knots are formed as holes in [27], which represent a similar case as a dead knot configuration. Then the samples are loaded under tension with a stress of 1 MPa. Global stress concentrations in the applied tensile stress direction are combined in Equ. (9) with the knot size areas at the location where the specific stress concentration occurs. Resulting stress concentration factors are calculated, where σ_{sim} describes the maximum tensile stress from simulations around the knot in global longitudinal board direction, A_{knot} represents the largest total cross section area of the knot on its central axis and A_{total} is the cross section of the board.

$$\mathrm{SCF}_1 = \max\left(\sigma_{sim} \cdot \frac{\mathrm{A}_{knot}}{\mathrm{A}_{total}}\right) \tag{9}$$

For 200 randomly selected boards, the local stress components in the FCS σ_{loc}, including normal and shear stress, are compared to SCF_1 in Section 3.2.

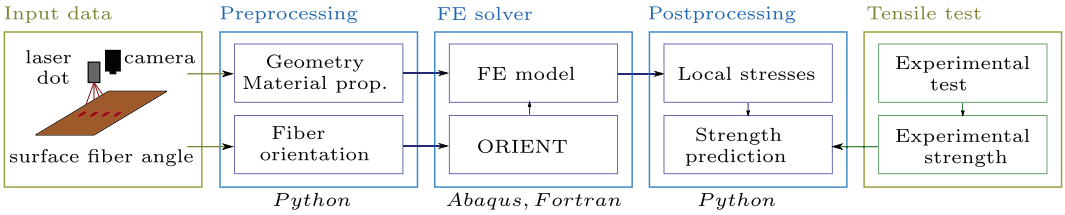

Fig. 5. Automatized workflow for calculating local stresses and global strength based on local material directions in the FE model and comparison according to tensile tests.

3. Results and discussion

The differences in local stress maxima are investigated in representative board sections to identify the impact of fiber deviations on the mechanical behavior. Local stress maxima are studied as a consequence of global unit tensile stress and relevant stress components are then used to predict the strength of the boards.

3.1. Evaluation of the numerical approach

The applied unit tensile stress in global longitudinal board direction σ_1 is distributed according to the local stress components in the direction of the local FCS. The global stress plot of a simulated tensile test for an example board with a knot is presented in Fig. 6, where the colors represent the stress in global x-direction and the stress distribution in the local FCS is expressed by vectors: σ_L represents the stress component in fiber direction shown by a vector in fiber direction and σ_R, σ_T, represent the stress components in radial, tangential directions, respectively shown with vectors in its corresponding direction. Due to the assumed constant ring angle of 0° along the board, shown in Fig. 1, the radial direction of boards without fiber deviation aligns with the global y-direction, and the tangential direction aligns with the global z-direction. Considering the comparatively larger horizontal fiber angles than diving angles, σ_T is more significant than σ_R for tensile loading in global x-direction and thus the focus of investigations in the following section are on σ_L and σ_T.

At locations without fiber deviation, the magnitude of global stress agrees with the local σ_L, whereas at locations with increased fiber deviation, the globally applied tensile stress in x-direction is distributed according to the transformed stiffness into the local stress components σ_L, σ_T, and a respectively small σ_R. Consequently, due to the transformed stiffness inside knots, the global stress in x-direction is close to zero, and distributed through y-/z-direction. Besides local normal stress components, local shear stress components develop due to the orthotropic material definition and may thus play a role for failure initiation in boards. Accordingly, shear components σ_{LT}, σ_{RT} are analyzed and are also taken into account as numerical parameters for tensile strength prediction.

Stress distribution in knots (knot zone (i)), in areas with large fiber deviations (fiber deviation zone (ii)) and in knot-free zones (clear wood zone (iii)) are investigated and are plotted in Fig. 7. The board sections shown in this figure, refer to the areas described in Section 2 and explain the influence of the transformed stiffness on the local stress components in example boards with knots (Fig. 7a) and boards without knots (Fig. 7b).

Scattering fiber measurements in the laser scanning data inside knots result in scattering stress distributions inside knots, thus fiber deviation regions around knots rather than regions inside knots are the focus of this study, similarly to [27].

Due to the stiffness properties in the ocal FCS, local tangential- (σ_T) and shear-stress (σ_{LT}, σ_{RT}) increases in regions with increasing fiber deviation, whereas local stress in fiber direction (σ_L) decreases in these areas. The σ_L parameter (Fig. 7a) reaches its maximum in the fiber deviation zone beside the knot in width direction similarly to concentrations of a plate with circular hole [27].

Inside knots, the applied tensile stress is partly redistributed to σ_T (or σ_R) or diverted to the fiber deviation zones around knots (Fig. 7a). A similar trend with increasing stress magnitudes in tangential direction σ_T is observed in fiber deviation regions for boards without knots (Fig. 7b). In the rest of the board, in the clear-wood zone, the stress in tangential direction tends to zero.

Longitudinal shear stress σ_{LT} and σ_{RT} distributions in boards are shown in Fig. 7. According to the fiber deviation, the material structure expressed by the transformation of the stress from the global to the local directions triggers also shear stress components, which increase or change in sign in fiber deviation regions corresponding to the change in fiber deviation.

In Fig. 7a, the location of maximum local stress components correspond to the experimental failure location on the longitudinal board axis, presented with red crosses in the figure. Numerical results are thus assumed to be closely related to the fracture initiation and location, also shown later in Fig. 8. In Fig. 7b, the location in longitudinal board direction of the fiber failure from the experiment with an observed angle of 10° corresponds approximately

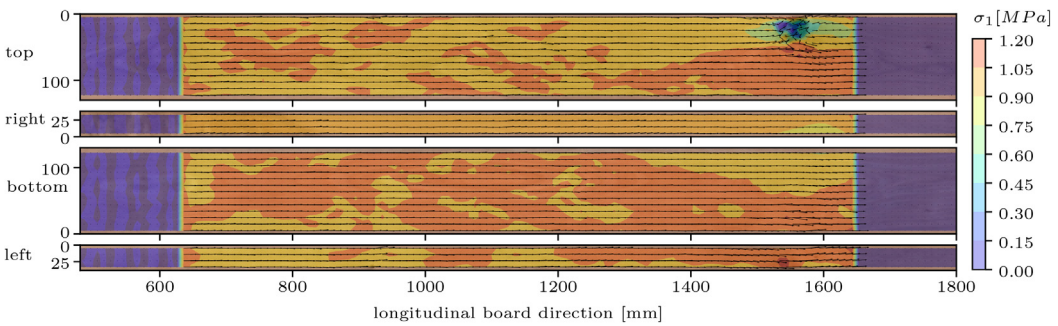

Fig. 6. Global stress distribution in test length (x-direction) of the experiment on the four surfaces of the board with knot. Vectors represent the local stress in longitudinal σ_L and tangential direction of the fibers σ_T.

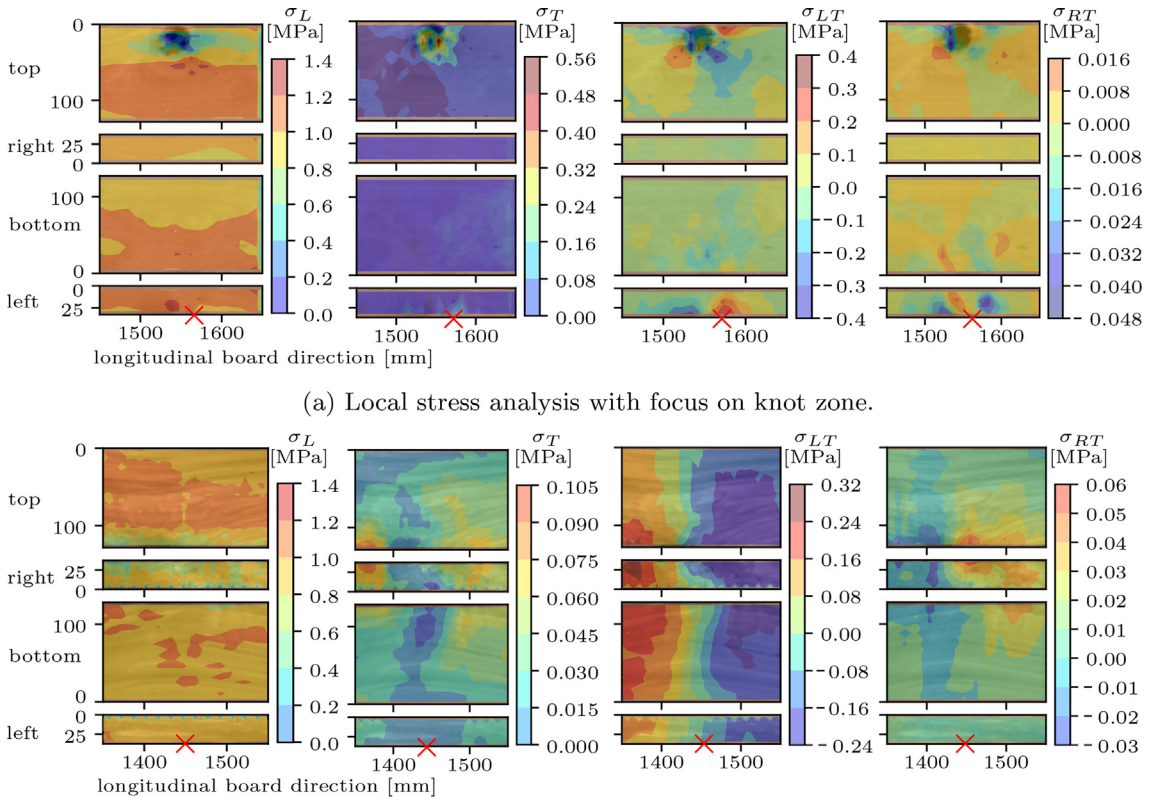

Fig. 7. Stress pattern in the local FCS is shown in longitudinal and tangential fiber direction for tensile stresses as well as for shear stresses. The red cross indicates the experimental failure location on the longitudinal board axis.

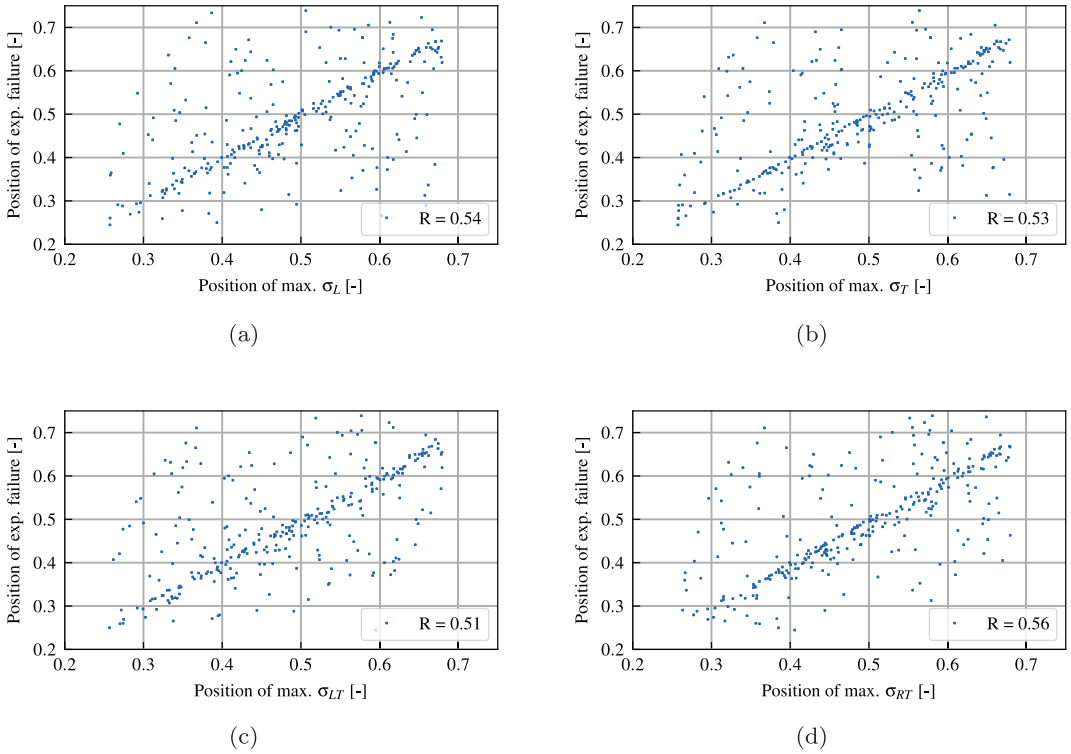

Fig. 8. Correlation of normalized failure location of the experiment (exp.) in global x-direction and normalized location of max. stress components in global x-direction.

with the location of especially longitudinal shear stress component σ_{LT}. The correlation between the normalized experimental failure location and the normalized max. numerical stress location in global x-direction is visualized for all boards in Fig. 8. The relation between failure locations are presented by means of the Pearson correlation coefficient, and values between R = 0.51 and R = 0.56 are reached. The experimental failure initiation location was observed after the experiment and might involve inaccuracies causing this scattering relation.

3.2. Strength prediction

3.2.1. Single regression analysis

Fig. 9 shows the correlation of single normal and shear stress components to the experimental strength f_t.

Together with the correlation matrix presented in Table 3, an inverse relation is shown between numerical stress components and the experimental tensile strength parallel to the grain. Strength prediction is performed with single maximum local stress components $\sigma_L, \sigma_T, \sigma_{LT}, \sigma_{RT}$ according to nonlinear functions. The exponential and potential regression equations represent the relation to strength and are thus evaluated. Both linear as well as nonlinear sets of equations are presented in Equ. (10)-(12).

$$f_{i,lin} = a_{i,lin} \cdot \sigma_i + b_{i,lin} \tag{10}$$

$$f_{i,exp} = a_{i,exp} \cdot e^{b_{i,exp} \cdot \sigma_i} + c_{i,exp} \tag{11}$$

$$f_{i,pot} = a_{i,pot} \cdot \sigma_i^{b_{i,pot}} + c_{i,pot} \tag{12}$$

Where $f_{i,lin}, f_{i,exp}, f_{i,pot}$ represent the predicted tensile strength based on numerical simulations, σ_i are the numerical stress components in $i = L, T, LT, RT$ directions and a_i, b_i, c_i are the constants, presented in Table 4. The coefficient of determination for each single regression analysis is summarized in Table 4.

The results of single regression analysis between the maximum stress in local fiber direction, σ_L, and the tensile strength is shown in Fig. 9a. Maximum stress magnitudes of 1 MPa to 4 MPa are obtained for σ_L parameter depending on estimated fiber deviations inside boards, as described in Section 3.1. The convergence to the numerical tensile stress of 1 MPa is shown in Fig. 9a, represented with the nonlinear potential and exponential function for σ_L. In this case, the highest coefficient of determination, $R^2 = 0.52$, is obtained for both exponential as well as power function. It is also shown in this graph that, due to the high natural scatter of the material, high scatter in strength exists even in boards without imperfections.

A similar behavior is shown in Fig. 9b for the stress component perpendicular to the fiber direction. It can be seen in this figure, that smaller stresses are obtained in the tangential direction, relative to the approximately ten times smaller stiffness values in this direction. By relating the numerical stress component σ_T to the tensile strength from the tests, the coefficient of determination of $R^2 = 0.61$ is obtained, when using the nonlinear functions.

In Fig. 9c,d, shear stresses of boards are shown and their relations to the measured tensile strength are outlined. To be able to understand the role of these stress components in the model, the position of shear failure as well as the type of failure in the experimental tests are investigated. The position of shear failure in the experimental tests is observed to be in good agreement with the positions of maximum σ_{LT} from simulations as shown in Fig. 7 for two exemplary cases and in Fig. 8,d for all 407 samples. As a single stress component, σ_{LT} represents an almost linear relation to the tensile strength with the coefficient of determination of $R^2 = 0.60$. The prediction quality improves slightly to $R^2 = 0.63$ when using an exponential function. A similar relation is described by the shear stress σ_{RT} which is characterized by the exponential function with $R^2 = 0.62$.

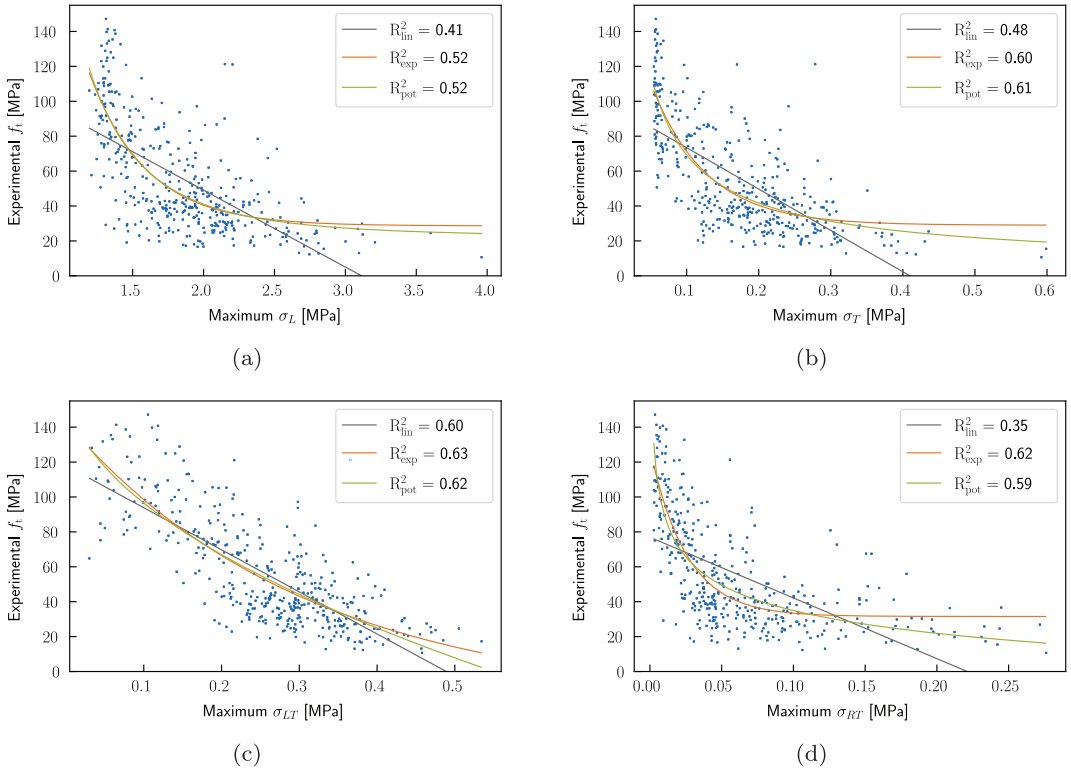

Fig. 9. Correlation of maximum local stresses $\sigma_L, \sigma_T, \sigma_{LT}, \sigma_{RT}$ from simulation to experimental tensile strength in single regression analysis for n = 407 samples. Coefficients of determination are given for linear and nonlinear functions.

Table 3
Correlation matrix with Pearson's correlation coefficient between the single stress components and the strength for the whole dataset of n = 407 boards.

	σ_L	σ_T	σ_{LT}	σ_{RT}	f_t
σ_L	1	0.84	0.74	0.73	−0.64
σ_T	0.84	1	0.83	0.73	−0.69
σ_{LT}	0.74	0.83	1	0.64	−0.77
σ_{RT}	0.73	0.84	0.64	1	−0.60
f_t	−0.64	−0.69	−0.77	−0.60	1

Table 4
Constants and coefficients of determination from single regression analysis expressed in Eqs. (10)-(12).

i	σ_i	$a_{i,lin}$	$b_{i,lin}$	$a_{i,exp}$	$b_{i,exp}$	$c_{i,exp}$	$a_{i,pot}$	$b_{i,pot}$	$c_{i,pot}$	R^2_{lin}	$R^2_{exp.}$	R^2_{pot}
1	$\sigma_{L,max}$	137.2	−44.1	1700.9	−2.5	28.6	169	−3.15	22.1	0.41	0.52	0.52
2	$\sigma_{T,max}$	97.1	−236.9	156.8	−13.1	29	11.5	−0.8	2.3	0.48	0.60	0.61
3	$\sigma_{LT,max}$	118	−241.2	161	−3.2	−18.3	−225.3	0.5	165.9	0.60	0.63	0.62
4	$\sigma_{RT,max}$	76.9	−347.7	96	−39.2	31.5	89	−0.2	−92.6	0.35	0.62	0.59
5	SCF_1	82.8	−7.5	80.6	−0.1	0	81.3	−0.5	0	0.37	0.43	0.52

Generally, single maximum local stress components show a promising correlation to the experimental strength. Shear stress σ_{LT} improves the quality of tensile strength predictions by 26% compared to normal stress in fiber direction σ_L as a single predictor.

However, it needs to be considered that the strength of such material can not be associated with only one specific local stress component and multiple stress components may play a role in predicting the strength of the material.

3.2.2. Multiple regression analysis

By analyzing the failure modes and locations of the samples in the experiments, an interaction of shear and normal stress failure is documented. Thus, the combination of normal stresses, can be enhanced for representing the stress interaction and consequent failure initiation, with shear components for a higher accuracy of strength prediction.

Considering possible combinations of local normal and shear stress components together in a nonlinear multiple regression analysis may improve the quality of tensile strength prediction. Table 5 presents possible combinations of stresses together with their coefficient of determination values from regression analysis with tensile strength.

The nonlinear regression equation for this analysis, considering the exponential function of single local stress components is presented in Equ. (13).

$$f_{j,exp} = \sum_{i=1}^{n} a_i \cdot e^{b_i \cdot \sigma_i} + c_i \tag{13}$$

Where $f_{j,exp}$ represents the predicted tensile strength based on numerical simulations, σ_i are the numerical stress components in $i = L, T, LT, RT$ directions and a_i, b_i, c_i are the constants according to n considered stress components, presented in Table 5. The coefficient of determination for each multiple regression analysis is summarized in Table 5.

Since shear components exclusively present good single predictors for tensile strength, on the left side of Fig. 10, the multiple relation analysis is performed considering the relation of these components with the actual tensile strength of the boards. By using these components together in a multiple regression analysis, a coefficient of determination of $R^2 = 0.69$ is reached. In comparison, combination of all relevant local stresses from simulations $\sigma_L, \sigma_T, \sigma_{LT}, \sigma_{RT}$, shown in Fig. 10 on the right side, relates similarly well to experimental tensile strength and reaches the maximum coefficient of determination of $R^2 = 0.70$.

For the validation of the method, the developed approach is compared to the studies presented in Section 2.4. Rais et al. [19], based the prediction approach on $SOG_{3D,150mm}$ and conducted the analysis on the same set of boards with the same surface fiber angle measurements. The analytical approach in [19] showed slightly lower results in predicting tensile strength with $R^2 = 0.61$ as the results based on multiple influence of single stress parameters in this study with $R^2 = 0.70$ shown in Fig. 10.

Furthermore, a random set of 200 samples is selected from this data set and the simulations are run to extract the stress concentration factor SCF_1, described in Section 2.4. The results of a single regression analysis show a relation of $R^2 = 0.52$ to experimental strength. This result is comparable to the predicted strength from linear regression analysis of the numerical normal stress parameters, σ_L extracted from the current study, with similar coefficients of determination of $R^2 = 0.52$. Due to the fact that shear forces play a decisive role, a multiple regression analysis combining maximum

Table 5
Constants and coefficients of determination from multiple regression analysis expressed in Eqs. (13).

j	σ_L	σ_T	σ_{LT}	σ_{RT}	$a_{i,1}$	$b_{i,1}$	$a_{i,2}$	$b_{i,2}$	$a_{i,3}$	$b_{i,3}$	$a_{i,4}$	$b_{i,4}$	c_i	R^2
1	x	x			−257	−80.0	156.8	−13.1	-	-	-	-	29	0.60
2	x		x		252	−1.9	122	−3.5	-	-	-	-	−7.2	0.64
3	x			x	95.3	−0.8	76.8	−45.1	-	-	-	-	15.2	0.64
4		x	x		98	−18.9	114.4	−2.2	-	-	-	-	−19.7	0.66
5		x		x	72.9	−10.7	55.9	−39.3	-	-	-	-	25.6	0.67
6			x	x	102.5	−2.9	51.6	−39	-	-	-	-	−14.2	0.69
7	x	x	x		−1.4	0.7	108.1	−22.2	101.7	−2.6	-	-	0.3	0.67
8	x		x	x	−1	0.8	91.5	−2.8	50.6	−41.5	-	-	1.2	0.69
9		x	x	x	58.5	−21.0	93.8	−1.8	41.6	−34.8	-	-	−21	0.70
10	x	x	x	x	3661	0.0	59	−22	41.3	−35.6	89.8	−1.9	−3675	0.70

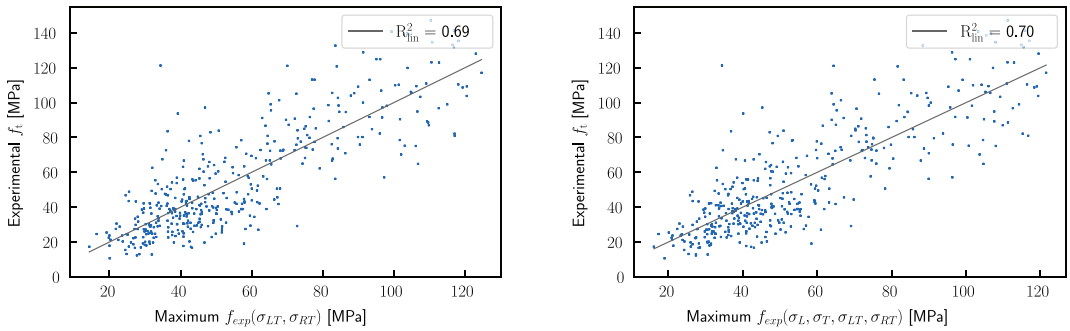

Fig. 10. Strength prediction based on the exponential combination of local stresses from simulations $\sigma_L, \sigma_T, \sigma_{LT}, \sigma_{RT}$. Correlation of predicted strength and experimental strength in multiple regression analysis for n = 407 European beech samples.

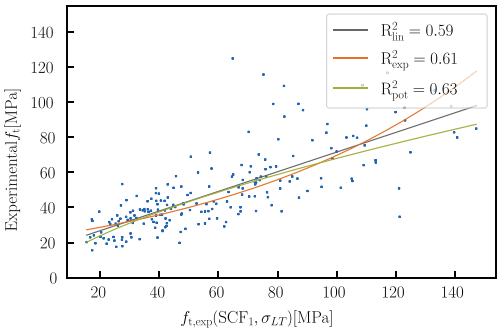

Fig. 11. Correlation of predicted strength, based on SCF_1 and the longitudinal shear stress, in a multiple regression analysis for n = 200 European beech samples.

shear stresses and SCF_1 in a nonlinear regression analysis predicts the tensile strength with a maximum $R^2 = 0.63$ as shown in Fig. 11.

In conclusion, the results are related to the State of the Art in the literature. A regression analysis using the E_{stat} with the bending strength provided a value of 0.71 for spruce boards [40]. By performing the dynamic measurements and consideration of the heterogeneities, Olsson et al. [41] came up with a coefficient of determination of 0.75 for bending strength predictions. Lukacevic et al. [42] provided a method that considers quadratically weighted knot information on board surfaces. This parameter in a regression analysis with the bending strength gave a high coefficient of determination of 0.76. Studies on tensile strength are relatively limited. In the same study [42], a value of $R^2 = 0.92$ was provided for spruce boards, considering the knot-area-ratio and fiber-deviation-area-ratio for 29 spruce samples. However, it is expected that the correlation reduces when the number of samples are increased and the heterogeneities cover a higher scatter. Khaloian and van de Kuilen [43] provided a virtual method by considering the numerical stress concentration factors ($SCF_{1,2,3}$) and the virtual dynamic $E_{dyn.}$ in a nonlinear multiple regression analysis with tensile strength with $R^2 = 0.71, 0.66$ and 0.59 for spruce, Douglas fir and beech, respectively. As shown here, different approaches have been developed to predict the strength of wood. However, most of the studies took into account the parameters from dynamic measurements, which are strong single predictors for strength. This study introduces solely a methodology for direct transformation of the laser-scan measurements into a finite element model that can further be analyzed for extraction of IPs for tensile strength predictions. At this stage, analyzing single stress components with a coefficient of determination of $R^2 = 0.70$ shows the capability of the developed method for strength prediction and for further numerical analysis.

4. Conclusion & outlook

Recent research has found robust links between local grain slope and strength, even when the mechanical behavior of the board is ignored. Therefore, this study presents a numerical approach for direct transformation of the laser scanning surface data into a 3D FE model for tensile strength predictions, where local material features can be automatically transferred into a deterministic numerical model.

The local FCSs were defined in a discretized way employing industrial laser scanning fiber angles from four surfaces into local stiffness properties in a FE model. In terms of fiber deviation inside the board and implementation of the pith position, the model includes simplifications. In this way, the fiber orientation on the surfaces was linearly interpolated into the board thickness direction. Because of the unknown pith location along the board solely based on the end-grain images, a constant ring angle of 0° was assumed along the board. Further modification of the implemented simplifications in the current numerical model for future models may result in more accurate representation of local material properties.

Experimental tensile testing data on all European beech boards was used for validation. In the elastic material range, maximum local stress components in the normal direction, as well as the shear stress components, were extracted as numerical strength predictors. By using these components in a single regression analysis with tensile strength the highest coefficient of determination ($R^2 = 0.63$) was obtained for the shear stress component σ_{LT}.

For the interpretation of the output, the interaction of the aforementioned local maximum stress components in different directions was processed mathematically with multiple regression analysis. An improvement of numerical strength prediction was observed by a statistical combination of normal stress components with shear stress components ($R^2 = 0.70$).

Numerical modeling based on local fiber orientation not only improves strength predictions, but also provides a better understanding of the mechanical behavior of boards with local heterogeneities. The introduced model is applicable for different board geometries and different wood species and may provide the basis for a more sophisticated analysis of failure initiation beyond statistical interpretation. The accuracy of strength prediction could be possibly further improved by using a phenomenological combination of multiple stress factors in combined stress states expressed by specific failure criteria, which take into account the different strength in different directions.

Declaration of Competing Interest

The authors declare that they have no known competing financial interests or personal relationships that could have appeared to influence the work reported in this paper.

Acknowledgements

We thank Microtec for the laser scanning data and Martin Bacher for the support during this work. Additionally we thank the German Research Foundation (DFG) through TUM International Graduate School of Science and Engineering (IGSSE), GSC81 for support of the project "FaiMONat - Multi-fidelity Failure Modeling and Optimization for natural Fiber Structures in Complex Environments".

References

[1] J. Nyström, Automatic measurement of fiber orientation in softwoods by using the tracheid effect, Comput. Electron. Agric. 41 (1–3) (2003) 91–99, https://doi.org/10.1016/S0168-1699(03)00045-0.
[2] B. Besseau, G. Pot, R. Collet, J. Viguier, Influence of wood anatomy on fiber orientation measurement obtained by laser scanning on five European species, J. Wood Sci. 66 (74) (2020), https://doi.org/10.1186/s10086-020-01922-y.
[3] P. Matthews, J.F. Soest, Method for determining localized fiber angle in a three dimensional fibrous material, US patent (1986).
[4] V. Daval, G. Pot, M. Belkacemi, F. Meriaudeau, R. Collet, Automatic measurement of wood fiber orientation and knot detection using an optical system based on heating conduction, Opt. Exp. 23 (26) (2015) 33529–33539, https://doi.org/10.1364/OE.23.033529.
[5] M. Norimoto, T. Yamada, The dielectric properties of wood: On the dielectric properties of the chemical constituents of wood and the dielectric anisotropy of wood, Wood Res. Inst. Kyoto Univ. 51 (12) (1972) 31–43.
[6] S.M. Cramer, K.A. McDonald, Predicting lumber tensile stiffness and strength with local grain angle measurements and failure analysis, Wood Fiber Sci. 21 (1) (1989) 393–410.
[7] T. Ehrhart, R. Steiger, A. Frangi, A non-contact method for the determination of fibre direction of European beech wood (*Fagus sylvatica* L.), Eur. J. Wood Wood Prod. 76 (3) (2018) 925–935, https://doi.org/10.1007/s00107-017-1279-3.
[8] J.A. Huber, O. Broman, M. Ekevad, J. Oja, L. Hansson, A method for generating finite element models of wood boards from x-ray computed tomography scans, Comput. Struct. 260 (106702) (2022), https://doi.org/10.1016/j.compstruc.2021.106702.
[9] A. Khaloian, W. Gard, J. van de Kuilen, 3D FE-numerical modelling of growth defects in medium dense european hardwoods, in: Proceedings of the 6th International Scientific Conference on Hardwood, National Ressources Institute Finland, Helsinki, 2017.
[10] S. Ormarsson, H. Dahlblom, H. Petersson, A numerical study of the shape stability of sawn timber subjected to moisture variation, part 1: Theory, Wood Sci. Technol. 32 (5) (1998) 325–334.
[11] A. Olsson, J. Oscarsson, E. Serrano, B. Källsner, M. Johansson, B. Enquist, Prediction of timber bending strength and in-member cross-sectional stiffness variation on the basis of local wood fibre orientation, Eur. J. Wood Wood Prod. 71 (3) (2013) 319–333, https://doi.org/10.1007/s00107-013-0684-5.
[12] J. Oscarsson, A. Olsson, B. Enquist, Localized modulus of elasticity in timber and its significance for the accuracy of machine strength grading, Wood Fiber Sci. 46 (4) (2014) 489–501.
[13] M. Hu, M. Johansson, A. Olsson, J. Oscarsson, B. Enquist, Local variation of modulus of elasticity in timber determined on the basis of non-contact deformation measurement and scanned fibre orientation, Eur. J. Wood Wood Prod. 73 (1) (2014) 17–27, https://doi.org/10.1007/s00107-014-0851-3.
[14] M. Hu, A. Briggert, A. Olsson, M. Johansson, J. Oscarsson, H. Säll, Growth layer and fibre orientation around knots in Norway spruce: a laboratory investigation, Wood Sci. Technol. 52 (1) (2018) 7–27, https://doi.org/10.1007/s00226-017-0952-3.
[15] A. Briggert, A. Olsson, J. Oscarsson, Three-dimensional modelling of knots and pith location in Norway spruce boards using tracheid-effect scanning, Eur. J. Wood Wood Prod. 74 (5) (2016) 725–739, https://doi.org/10.1007/s00107-016-1049-7.
[16] T. Habite, A. Olsson, J. Oscarsson, Automatic detection of pith location along Norway spruce timber boards on the basis of optical scanning, Eur. J. Wood Wood Prod. 78 (6) (2020) 1061–1074, https://doi.org/10.1007/s00107-020-01558-1.
[17] A. Briggert, M. Hu, A. Olsson, J. Oscarsson, Tracheid effect scanning and evaluation of in-plane and out-of-plane fiber direction in Norway spruce timber, Wood Fiber Sci. 50 (4) (2018) 411–429, https://doi.org/10.22382/wfs-2018-053.
[18] F. Hunger, J. van de Kuilen, Slope of grain measurement: a tool to improve machine strength grading by detecting top ruptures, Wood Sci. Technol. 52 (3) (2018) 821–838, https://doi.org/10.1007/s00226-018-1000-7.
[19] A. Rais, M. Bacher, A. Khaloian-Sarnaghi, M. Zeilhofer, A. Kovryga, F. Fontanini, T. Hilmers, M. Westermayr, M. Jacobs, H. Pretzsch, J.W.G. van de Kuilen, Local 3D fibre orientation for tensile strength prediction of European beech timber, Constr. Build. Mater. 279 (2021), https://doi.org/10.1016/j.conbuildmat.2021.122527.
[20] G. Kandler, M. Lukacevic, J. Füssl, An algorithm for the geometric reconstruction of knots within timber boards based on fibre angle measurements, Constr. Build. Mater. 124 (2016) 945–960, https://doi.org/10.1016/j.conbuildmat.2016.08.001.
[21] C. Foley, Modeling the effects of knots in structural timber, Dissertation, Lund University, Lund, 2003.
[22] S.M. Cramer, J.R. Goodman, Failure modeling: A basics for strength prediction of lumber, Wood Fiber Sci. 18 (1986) 446–459.
[23] J.R. Goodman, J. Bodig, Tension behavior of wood - an anisotropic, inhomogeneours material, Structural research report no. 32, Colorado State University (1980).
[24] P. Guindos, M. Guaita, A three-dimensional wood material model to simulate the behavior of wood with any type of knot at the macro-scale, Wood Sci. Technol. 47 (2013) 585–599, https://doi.org/10.1007/s00226-012-0517-4.
[25] P. Guindos, Method for the integral calculation of the fiber orientation and the fundamental material properties of softwood logs and lumber, Holzforschung 70 (10) (2016) 981–991, https://doi.org/10.1515/hf-2015-0197.
[26] R. Lang, M. Kaliske, Description of inhomogeneities in wooden structures: modelling of branches, Wood Sci. Technol. 47 (5) (2013) 1051–1070, https://doi.org/10.1007/s00226-013-0557-4.
[27] A. Khaloian Sarnaghi, J.W.G. van de Kuilen, Strength prediction of timber boards using 3D FE-analysis, Constr. Build. Mater. 202 (2019) 563–573, https://doi.org/10.1016/j.conbuildmat.2019.01.032.
[28] C. Hackspiel, K. Borst, M. Lukacevic, A numerical simulation tool for wood grading model development, Wood Sci. Technol. 48 (3) (2014) 633–649, https://doi.org/10.1007/s00226-014-0629-0.
[29] M. Lukacevic, J. Füssl, Numerical simulation tool for wooden boards with a physically based approach to identify structural failure, Eur. J. Wood Wood Prod. 72 (4) (2014) 497–508, https://doi.org/10.1007/s00107-014-0803-y.
[30] M. Lukacevic, G. Kandler, M. Hu, A. Olsson, J. Füssl, A 3D model for knots and related fiber deviations in sawn timber for prediction of mechanical properties of boards, Mater. Des. 166 (2019) 107617, https://doi.org/10.1016/j.matdes.2019.107617.
[31] K. Frühwald, G. Schickhofer, Strength grading of hardwoods, in: 8th World Conference on Timber Engineering, WCTE 2004, 2004, pp. 675–679.
[32] G. Ravenshorst, Species independent strength grading of structural timber, Technische Universitet Delft, Delft, Disseratation, 2015.
[33] A. Rais, E. Ursella, E. Vicario, F. Giudiceandrea, The use of the first industrial X-ray CT scanner increases the lumber recovery value: case study on visually strength-graded Douglas-fir timber, Annals Forest Sci 74 (2) (2017) 1–9, https://doi.org/10.1007/s13595-017-0630-5.
[34] H. Pretzsch, P. Biber, G. Schütze, J. Kemmerer, E. Uhl, Wood density reduced while wood volume growth accelerated in Central European forests since 1870, For. Ecol. Manage. 429 (2018) 589–616, doi:10.1016/j.foreco.2018.07.045.
[35] CEN, EN 408:2012–1+A1:2012, timber structures - structural timber and glued laminated timber - determination of some physical and mechanical properties, 2012.
[36] CEN, EN 384:2016+A1:2018, structural timber - determination of characteristic values of mechanical properties and density, 2019.
[37] P. Matthews, B.H. Beech, Method and apparatus for detecting timber defects, US patent (1976).
[38] P. Niemz, W.U. Sonderegger, Holzphysik: Physik des Holzes und der Holzwerkstoffe, Fachbuchverlag Leipzig im Carl Hanser Verlag, München (2017), https://doi.org/10.3139/9783446445468.
[39] L.P. Kollar, G.S. Springer, Mechanics of composite structures, Cambridge University Press (2003), https://doi.org/10.1017/CBO9780511547140.
[40] J. Oscarsson, Strength grading of structural timber and EWP laminations of Norway spruce: Development potentials, Dissertation, Linneaeus University, Linneaeus, 2012.
[41] A. Olsson, J. Oscarsson, M. Johansson, B. Källsner, Prediction of timber bending strength on basis of bending stiffness and material homogeneity assessed from dynamic excitation, Wood Sci. Technol. 46 (2012) 667–683, https://doi.org/10.1007/s00226-011-0427-x.
[42] M. Lukacevic, J. Füssl, J. Eberhardsteiner, Discussion of common and new indicating properties for the strength grading of wooden boards, Wood Sci. Technol. 49 (3) (2015) 551–576, https://doi.org/10.1007/s00226-015-0712-1.
[43] A. Khaloian Sarnaghi, J.W.G. van de Kuilen, An advanced virtual grading method for wood based on surface information of knots, Wood Sci. Technol. 53 (3) (2019) 535–557, https://doi.org/10.1007/s00226-019-01089-w.